

**HIGH CYCLE FATIGUE
CRACK MODELING AND ANALYSIS
FOR DECK TRUSS FLOORING
CONNECTION DETAILS**

Final Report

**State Planning and Research
Project Number 5280**

by

Anthony H. DePiero
Graduate Research Assistant

Robert K. Paasch, Ph. D.
Professor of Mechanical Engineering

Prepared for

Oregon Department of Transportation
Research Unit
Salem, Oregon 97310

and

Federal Highway Administration
Washington, D. C. 20560

July 1997

SI* (MODERN METRIC) CONVERSION FACTORS

APPROXIMATE CONVERSIONS TO SI UNITS				APPROXIMATE CONVERSIONS FROM SI UNITS			
Symbol	When You Know	Multiply By	To Find	Symbol	When You Know	Multiply By	To Find
LENGTH							
in	inches	25.4	millimeters	mm	millimeters	0.039	inches
ft	feet	0.305	meters	m	meters	3.28	feet
yd	yards	0.914	meters	m	meters	1.09	yards
mi	miles	1.61	kilometers	km	kilometers	0.621	miles
AREA							
in ²	square inches	645.2	millimeters squared	mm ²	millimeters squared	0.0016	square inches
ft ²	square feet	0.093	meters squared	m ²	meters squared	10.764	square feet
yd ²	square yards	0.836	meters squared	m ²	hectares	2.47	acres
ac	acres	0.405	hectares	ha	kilometers squared	0.386	square miles
mi ²	square miles	2.59	kilometers squared	km ²			
VOLUME							
fl oz	fluid ounces	29.57	milliliters	mL	milliliters	0.034	fluid ounces
gal	gallons	3.785	liters	L	liters	0.264	gallons
ft ³	cubic feet	0.028	meters cubed	m ³	meters cubed	35.315	cubic feet
yd ³	cubic yards	0.765	meters cubed	m ³	meters cubed	1.308	cubic yards
NOTE: Volumes greater than 1000 L shall be shown in m ³ .							
MASS							
oz	ounces	28.35	grams	g	grams	0.035	ounces
lb	pounds	0.454	kilograms	kg	kilograms	2.205	pounds
T	short tons (2000 lb)	0.907	megagrams	Mg	megagrams	1.102	short tons (2000 lb)
TEMPERATURE (exact)							
°F	Fahrenheit temperature	5(F-32)/9	Celsius temperature	°C	Celsius temperature	1.8 + 32	Fahrenheit



* SI is the symbol for the International System of Measurement (4-7-94 jbp)

DISCLAIMER

This document is disseminated under the sponsorship of the Oregon Department of Transportation and the United States Department of Transportation in the interest of information exchange. The State of Oregon and the United States Government assume no liability of its contents or use thereof.

The contents of this report reflect the views of the authors, who are responsible for the facts and the accuracy of the data presented herein. The contents do not necessarily reflect the official policies of the Oregon Department of Transportation or the United States Department of Transportation.

The State of Oregon and the United States Government do not endorse products of manufacturers. Trademarks or manufacturer's names appear herein only because they are considered essential to the object of this document.

This report does not constitute a standard, specification, or regulation.

**HIGH CYCLE FATIGUE CRACK MODELING AND ANALYSIS FOR
DECK TRUSS FLOORING CONNECTION DETAILS**
Final Report

TABLE OF CONTENTS

1.0	INTRODUCTION	1
2.0	PROBLEM SPECIFICATION	3
3.0	BACKGROUND AND THEORY	7
3.1	BACKGROUND	7
3.2	FINITE ELEMENT ANALYSIS	8
3.3	FATIGUE	10
4.0	LOADING ANALYSIS	15
4.1	STRINGER LOADING ANALYSIS	15
4.2	GLOBAL FEA MODEL	17
4.3	RESULTS	21
5.0	DEFLECTION AND STRESS ANALYSIS	25
5.1	CLIP ANGLE DEFLECTION AND STRESS ANALYSIS	25
5.2	2D FEA MODEL	29
5.3	3D FEA MODEL	30
5.4	RESULTS	32
6.0	FATIGUE ANALYSIS	39
6.1	STRESS-LIFE	39
6.2	LINEAR-ELASTIC FRACTURE ANALYSIS	40
6.3	REMAINING FATIGUE LIFE	42
6.4	RESULTS	42
7.0	IDENTIFICATION METHODOLOGY	45
8.0	RETROFIT STRATEGIES	49

9.0	SUMMARY AND CONCLUSIONS	53
-----	-------------------------------	----

REFERENCES	55
------------------	----

APPENDICES

Appendix A:	STRINGER LOADING ANALYSIS
Appendix B:	GLOBAL FEA MODEL
Appendix C:	REINFORCED CONCRETE DECK ANALYSIS
Appendix D:	CLIP ANGLE DEFLECTION ANALYSIS
Appendix E:	CLIP ANGLE STRESS ANALYSIS
Appendix F:	2D FEA MODEL
Appendix G:	3D FEA MODEL
Appendix H:	STRESS-LIFE
Appendix I:	LINEAR-ELASTIC FRACTURE MECHANICS
Appendix J:	IDENTIFICATION METHODOLOGY

LIST OF TABLES

Table 5.1	COMPARISON OF INTERIOR PANEL CLIP ANGLE DEFLECTIONS FROM EACH ANALYSIS METHOD	34
Table 5.2	COMPARISON OF INTERIOR PANEL CLIP ANGLE MAXIMUM STRESS RANGE (KSI) RESULTS FROM EACH ANALYSIS METHOD	37
Table 5.3	CLIP ANGLE STRESS RANGE RESULTS FROM THE 3D FEA MODEL FOR BOTH THE NORTH AND SOUTHBOUND STRUCTURE	38

Table 6.1	ESTIMATED REMAINING LIFE (YEARS) OF THE DIFFERENT CLIP ANGLES CALCULATED USING THE STRESS-LIFE FATIGUE ANALYSIS	43
Table 6.2	ESTIMATED REMAINING LIFE (YEARS) OF THE DIFFERENT CLIP ANGLES CALCULATED USING LINEAR-ELASTIC FRACTURE MECHANICS	43
Table 8.1	EFFECTIVENESS OF THE FIVE RETROFIT STRATEGIES INVESTIGATED	51

LIST OF FIGURES

Figure 1.1	FLOW CHART OF THE PROJECT PHASES	2
Figure 2.1	DIAGRAM OF ONE SPAN OF THE SOUTHBOUND STRUCTURE OF THE WINCHESTER	3
Figure 2.2	TYPICAL STRINGER TO FLOOR BEAM CONNECTION DETAIL ASSEMBLY	4
Figure 2.3	CLIP ANGLE USED IN THE STRINGER TO FLOOR BEAM ASSEMBLIES ON THE WINCHESTER BRIDGE	4
Figure 2.4	CLIP ANGLE WITH A TYPICAL FATIGUE CRACK	5
Figure 3.1	THREE MODES OF CRACK DISPLACEMENT	13
Figure 4.1	SUGGESTED STANDARD FATIGUE TRUCK OUTLINED IN THE NCHRP REPORT 299	15
Figure 4.2	TOP VIEW DIAGRAM OF THE THREE STRINGERS THAT ARE ASSUMED TO CARRY THE AXLE LOAD IN THE STRINGER LOADING ANALYSIS	16
Figure 4.3	DIAGRAM OF THE LOADING AND BOUNDARY CONDITIONS USED IN THE STRINGER LOADING ANALYSIS	16
Figure 4.4	THREE STRINGERS AND TWO FLOOR BEAMS ON THE NORTHBOUND STRUCTURE OF THE WINCHESTER BRIDGE THAT HAD STRAIN GAGES INSTALLED	19

Figure 4.5	GRAPH OF THE STRINGER STRESS RANGES FROM THE GLOBAL FEA MODEL AND THOSE MEASURED EXPERIMENTALLY, LOADED WITH A KNOWN TRUCK WEIGHT	20
Figure 4.6	GRAPH OF THE STRINGER STRESS RANGES FROM THE GLOBAL FEA MODEL AND THOSE MEASURED EXPERIMENTALLY, UNDER RANDOM TRAFFIC LOADING	20
Figure 4.7	GRAPH OF THE STRINGER LOADS FOR THE NORTHBOUND STRUCTURE FOR BOTH THE STRINGER LOADING ANALYSIS AND THE GLOBAL FEA MODEL	22
Figure 4.8	GRAPH OF THE STRINGER LOADS FOR THE SOUTHBOUND STRUCTURE FOR BOTH THE STRINGER LOADING ANALYSIS AND THE GLOBAL FEA MODEL	22
Figure 4.9	GRAPH OF THE LOAD ON THE 2ND FROM MIDDLE STRINGER VS. THE DECK THICKNESS FROM THE GLOBAL FEA MODEL	23
Figure 5.1	STRINGER MODEL, ILLUSTRATING LOADING AND BOUNDARY CONDITIONS	25
Figure 5.2	TOP OF THE FLOOR BEAM LEG OF THE CLIP ANGLE MODELED AS A CANTILEVER BEAM	26
Figure 5.3	DIAGRAM OF CLIP ANGLE SHOWING THE CENTER OF ROTATION AND THE RELATIONSHIP OF F_R AND M_O	27
Figure 5.4	2D FEA MODEL OF THE TOP OF THE CLIP ANGLE ILLUSTRATING SIZE DIMENSIONS, BOUNDARY CONDITIONS, AND LOADING	29
Figure 5.5	EXAGGERATED DEFLECTION PLOT FROM THE 2D FEA MODEL OF AN INTERIOR PANEL CLIP ANGLE	33
Figure 5.6	EXAGGERATED DEFLECTION PLOT FROM THE 3D FEA MODEL OF AN INTERIOR PANEL CLIP ANGLE	33
Figure 5.7	FRINGE PLOT OF THE MAXIMUM PRINCIPAL STRESS FOR A INTERIOR PANEL CLIP ANGLE FROM THE 2D FEA MODEL	35

Figure 5.8	FRINGE PLOT OF THE MAXIMUM PRINCIPAL STRESS FROM THE 3D FEA MODEL USING THE FIXED ROTATION MODEL OF THE FLOOR BEAM	36
Figure 5.9	FRINGE PLOT OF THE MAXIMUM PRINCIPAL STRESS FROM THE 3D FEA MODEL USING THE FIXED TOP FLANGE MODEL OF THE FLOOR BEAM	36
Figure 7.1	LOAD ON THE 2ND FROM MIDDLE STRINGER VS. THE STRINGER SPACING	46
Figure 8.1	DRAWING OF THE RETROFIT STRATEGY TWO USED TO REPLACE DAMAGED CLIP ANGLES ON THE WINCHESTER BRIDGE IN 1994	50
Figure 8.2	DIAGRAM OF THE RETROFIT STRATEGY FIVE, GEOMETRIC STIFFENING	51



1.0 INTRODUCTION

The Oregon Department of Transportation (ODOT) is responsible for approximately 320 steel bridges, many of which have flooring system connection details that are fatigue prone. Over 20 structures have been found to have details with fatigue cracks. The majority of these bridges built prior to 1960, have details nearing the end of their fatigue life and will require increased inspection and repair over the next 10 to 20 years. Bridges on major routes require added attention since they can experience as many as 1 to 5 million significant load cycles per year. Some of these bridges have over 1000 connection details making the cost of inspection and repair very expensive.

The need to quantify the fatigue condition of these connection details is apparent. It is driven by the desire to limit inspection and to repair or replace only details with potential problems. The need exists to accurately assess the loading conditions and fatigue crack growth rate for the connection details and to develop a low cost field identification methodology to identify problem details. The current procedure is to repair only those connection details that currently contain visible fatigue cracks. Other connection details are left in service even though they may be nearing the end of their serviceable life. A more economic repair procedure could be implemented if there is detailed knowledge about which details are nearing the end of their fatigue life.

The goal of this research is to accurately assess the loading conditions and the fatigue crack growth rate for the connection details of a specific bridge, the Winchester Bridge on Interstate 5 in Roseburg, Oregon. Even though the analysis is being performed for this specific bridge, there is an expectation that the procedure, and to some degree, the results, can be applied to other bridges. Figure 1.1 shows a flowchart of the different phases of the project.

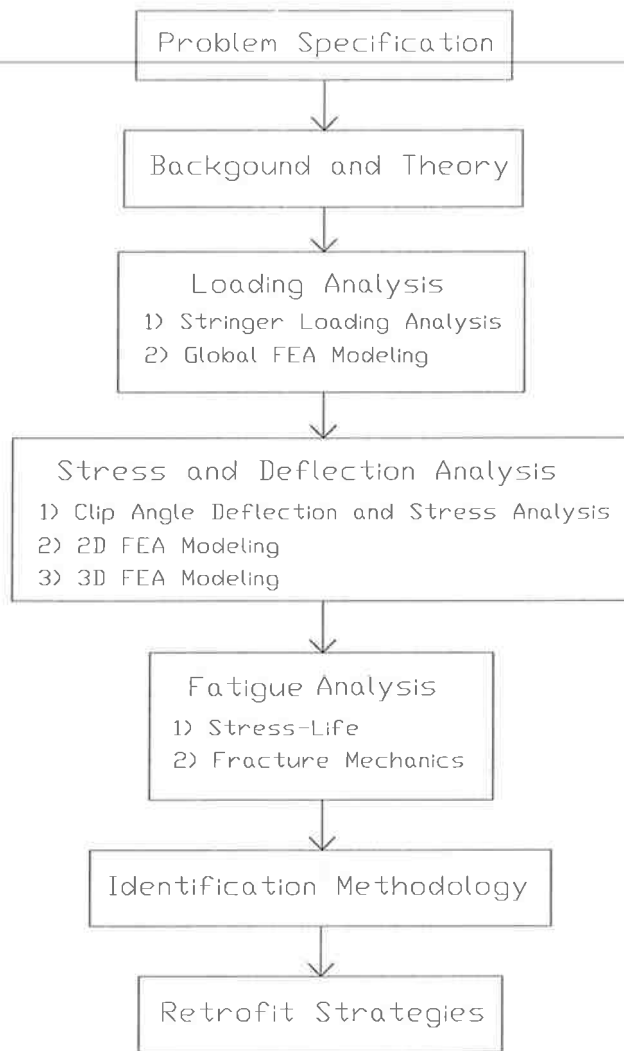


Figure 1.1 Flow chart of the project phases.

Problem specifications are discussed in Chapter 2; the specific bridge for study is identified and described. The Loading Analysis is addressed in Chapter 4 and includes a discussion of the two analysis methods used to determine the loading on the stringers (beams attached to connection details). In Chapter 5, Stress and Deflection Analysis, the deflections and stress ranges of the connection details are quantified. Detailed finite element models are used extensively in the both the Loading Analysis and the Deflection and Stress Analysis. Hand calculations are used to gain insight into and guide the development of the finite element models. Experimental data are used to validate the analysis. Chapter 6 covers the Fatigue Analysis and includes reviews of the two methods used for estimating the connection details' remaining life. The development of a low cost field identification methodology to identify problem connection details is discussed in Chapter 7. In Chapter 8 results are presented from the investigation of five retrofit strategies. The project is summarized in Chapter 9.

2.0 PROBLEM SPECIFICATION

The Winchester Bridge is a typical steel deck truss bridge under the responsibility of ODOT that has experienced high cycle fatigue problems in its flooring system connection details. For this reason, the Winchester Bridge was selected for study.

The Winchester Bridge, located on Interstate 5, five miles north of Roseburg, Oregon, spans the North Fork of the Umpqua River. The bridge has separate north and southbound structures that were constructed in 1953 and 1963, respectively. The two structures are very similar in their construction. Each structure is made of six, 140 foot steel deck truss spans. Figure 2.1 illustrates one span of the southbound structure without the reinforced concrete deck. The spans are separated by expansion joints

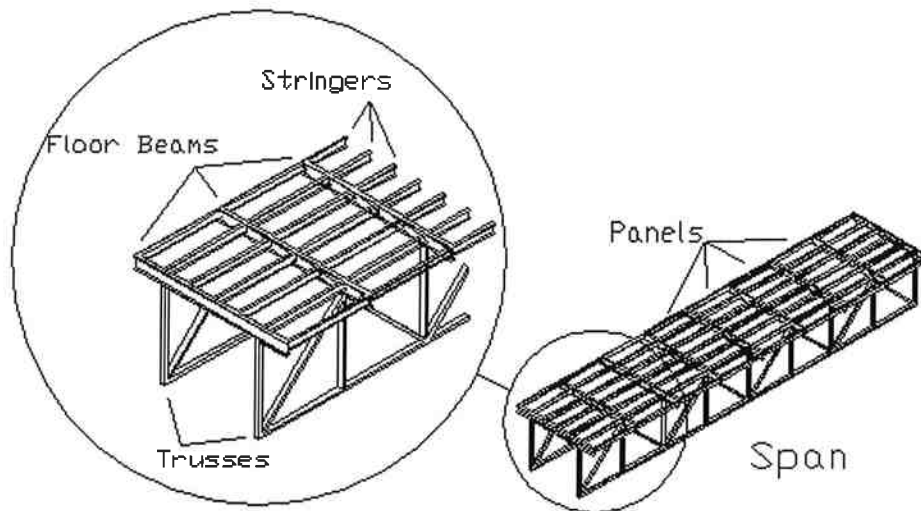


Figure 2.1 Diagram of one span of the southbound structure of the Winchester Bridge without the six inch concrete deck.

making them independent of one another. Each span is made up of a pair of steel trusses whose center lines are 20 feet apart. Each pair of trusses supports nine laterally oriented floor beams that are 17.5 feet apart. The sections between the floor beams are called “panels”. The northbound structure has five stringers in each panel running between the floor beams. The southbound structure has seven stringers in each panel. A six inch thick reinforced concrete deck lays on top of the floor beams and stringers. The north and southbound structures have slightly different size floor beams and stringers. In the northbound structure the floor beams are W24 x

76 wide flange steel beams and the stringers are W18 x 50 wide flange steel beams. In the southbound structure the floor beams are W27 x 84 wide flange steel beams and the stringers are W18 x 45 wide flange steel beams.

It is in the connection details (or clip angles) that connect the stringers to the floor beams that fatigue cracks have been found. Figure 2.2 shows a typical connection detail assembly.

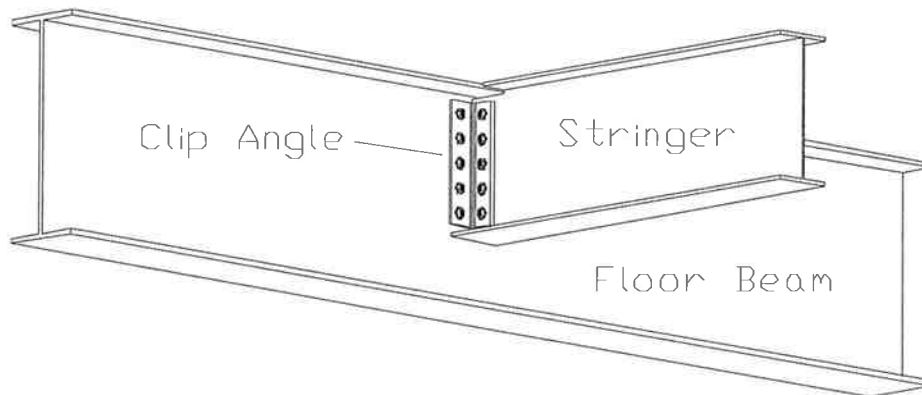


Figure 2.2 Typical stringer to floor beam connection detail assembly.

Figure 2.3 illustrates the clip angle used in the stringer to floor beam connection assemblies on the Winchester Bridge. The clip angles are connected to the stringers and floor beams using $\frac{7}{8}$

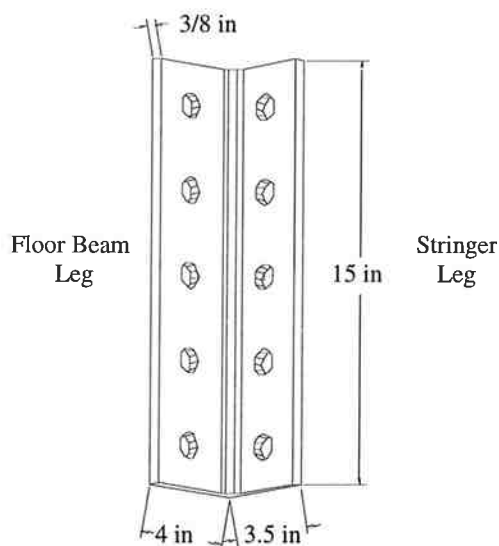


Figure 2.3 Clip angle used in the stringer to floor beam assemblies on the Winchester Bridge.

inch diameter rivets. Rivet holes are positioned 1.5 inches from the edges and spaced 3 inches apart on center.

The primary function of the clip angles is to transmit the shear from the stringer to the floor beam. Because they are riveted to both the stringer and floor beam, the angles are subjected to flexural stresses caused by the vertical deflection of the stringer under wheel loads. As the stringer deflects, the rotation of the end of the stringer subjects the connection detail to a flexural moment.

Fatigue cracks as long as four inches have been found in the clip angles. The cracks have been located at the corner of the clip angle running vertically from the top of the clip angle down. The fracture surface of the cracks have been oriented at an angle of approximately 45 degrees to the legs of the clip angle. Figure 2.4 illustrates a clip angle with a typical fatigue crack.

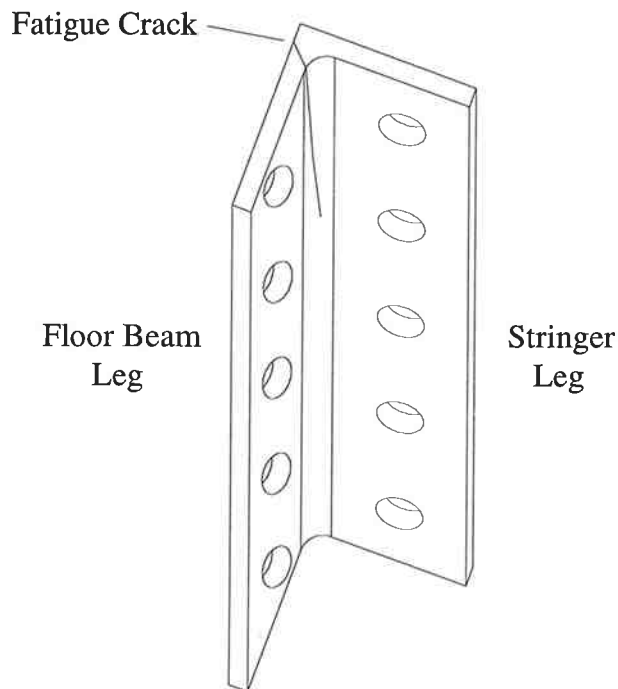


Figure 2.4 Clip angle with a typical fatigue crack.

In 1994, repair was conducted on both the north and southbound structures of the Winchester Bridge. Thirteen cracked clip angles were replaced on the southbound structure at a cost of \$16,384. Similar work was performed on the northbound structure at a cost of \$16,296.

The north and southbound structures of the Winchester Bridge are logical choices on which to perform a detailed analysis. The structures are typical steel deck truss bridges which have both had significant fatigue problems and experience a high number of load cycles per year. They are also crucial structures for the transportation of people and goods through the interstate corridor.

3.0 BACKGROUND AND THEORY

The first step in solving a problem is to first establish what research has already been performed that can assist in solving that problem. The examination of research performed on similar projects can give insight and help in understanding the problem currently being studied.

The connection angles in a study of railway bridge connection angles performed by Wilson of the University of Illinois [Wilson, 1940] are very similar to the clip angles used on the Winchester Bridge. A finite element analysis and field testing were performed by [Cao et al, 1996] on a Colorado State Route 224 bridge over the South Platte River near Commerce City. The National Cooperative Highway Research Program (NCHRP) Report 299, *Fatigue Evaluation Procedures for Steel Bridges* [Moses, et al, 1987] contains comprehensive fatigue evaluation procedures developed to guide the fatigue evaluation of existing bridges. The NCHRP Report 299, the study of the reinforced concrete deck, and Wilson's study on railway bridge connection details are discussed in the following section.

Basic principles and theory are used as tools in research. For this project the use and understanding of finite element analysis (FEA) and fatigue theory are very important. FEA and the FEA modeling tools used in this research, as well as three methods of fatigue analysis are reviewed in the following sections.

3.1 BACKGROUND

Fatigue in bridges has been a concern to the transportation community for many years. Studies of connection angles for stringers of railway bridges were performed in the late 1930's by Wilson and Coombe of the University of Illinois [Wilson, 1940] and [Wilson and Coombe, 1939]. Both computational analysis and fatigue testing were performed. The connection details that Wilson studied experience flexural stresses due to deformation of the bridge. There are two actions that contributed to these flexural stresses.

The first was the lengthening of the bottom chord of the truss with passage of a train. The stringers did not experience a corresponding change in length and since the floor beams are connected to both bottom chord and the stringers an axial force was produced and transmitted through the connection angles. One stress cycle was completed for each passage of a train.

The second action was the vertical deflection of the stringer under each set of wheels. The deflection rotated the end of the stringer and subjected the connection detail to a flexural moment. Stress cycles from this action were repeated for the passage of each car.

Wilson concluded that, because the stress in a flexural member varies as the square of the length, the stress state is much worse for connection details with short stiff legs than those with longer more flexible legs [Wilson, 1940].

Nine connection details of three different configurations were fatigue tested by repeatedly applying axial loads. The tests were designed to find the fatigue strengths of both connection angles and rivets [Wilson and Coombe, 1939].

The purpose of the study on the reinforced concrete bridge decks was to determine whether the top transverse reinforcing bars in the deck are necessary to sustain the negative bending moments and the tensile stresses seen in the top of the deck over the girders. The motivation for eliminating the top transverse reinforcing bars is that they are most susceptible to corrosion from deicing chemicals. [Cao, et al, 1996]

A finite element model was used in conjunction with experimental testing to determine the stress of the deck over the girders. Both the concrete deck and the girders were modeled. The concrete deck in the vicinity of the load points was modeled using a two layers of solid elements. The girders were modeled using 3D beam elements. Rigid beam elements were used to connect the nodes on the bottom of the deck to the centroid of the girders. In areas away from the load points equivalent beam elements were used to model the combination of the deck and the girders. [Cao, et al, 1996]

A substantial amount of research has been done to develop fatigue evaluation procedures for bridges. The National Cooperative Highway Research Program (NCHRP) Report 299, *Fatigue Evaluation Procedures for Steel Bridges* [Moses, et al, 1987] is a comprehensive report that outlines procedures for evaluating the fatigue condition of existing steel bridges. Loading issues, such as the proposed standard fatigue truck, impact, truck superposition, and cycles per truck passage, are discussed. The report contains methods for calculating moment ranges, stress ranges and the remaining fatigue life. Options for different levels of effort that reduce uncertainties and improve predictions of remaining life are presented. The evaluation procedures provided an effective guide to developing the analysis methods used in the project.

3.2 FINITE ELEMENT ANALYSIS

The finite element method, which was introduced in the late 1950's, is a type of computer simulation that is used to perform computational mechanics. The component of interest is first divided up into many small boxes or elements. The elements can have irregular shapes and conform closely to the shape of the component being modeled. The collection of elements forms a three-dimensional grid or mesh and makes the object look as though it is made of small building blocks. Nodes are points in the mesh where elements are connected. Discrete equations are used to mathematically couple adjacent nodes of the mesh to one another. Although the equations couple only adjacent nodes, they are derived from global balance laws. The following sections discuss the finite element method modeling tools that are used in the global FEA model, the 2D FEA model, and the 3D FEA model.

3.2.1 GLOBAL FEA MODELING

COSMOS/M was used to perform the finite element macro modeling. COSMOS/M is a modular, self-contained finite element system developed by Structural Research and Analysis Corporation [*COSMOS/M User's Guide*, 1992]. The module GEOSTAR was used as the mesh generator and post-processor. The STAR module was used for the linear static analysis of the deck structure. Other modules are available with a variety of different modeling capabilities.

3.2.2 2D FEA MODELING

The 2D modeling was performed using codes developed by the Methods Development Group at Lawrence Livermore National Laboratory (LLNL). MAZE was used to generate the mesh. It was developed as a mesh generator for the LLNL family of 2D FEA codes. [Hallquist, 1983]

NIKE2D was used to perform the analysis. This program is a nonlinear, implicit, 2D finite element code for solid mechanics. It uses a variety of elastic and inelastic material models. It has slide line algorithms that permit gaps, frictional sliding, and single surface contact along material interfaces. [Engelmann, 1991]

ORION was used to view the results generated by NIKE2D. It is an interactive color post-processor developed to view the results of the 2D FEA codes at LLNL. [Hallquist and Levatin, 1992]

3.2.3 3D FEA MODELING

Mesh generation for the 3D FEA model was performed using INGRID and later using TrueGrid. INGRID is a generalized 3D finite element mesh generator developed by the Methods Development Group at LLNL. It has the capability of generating complex geometrical models of nonlinear systems with beam, shell, and hexahedral elements. [Christon and Dovey, 1992]

TrueGrid is a highly interactive mesh generator for wide range of 3D FEA codes. It is similar to INGRID and will generate complex meshes using beam, shell, and hexahedral elements. It was developed by XYZ Scientific Applications, Inc. [*TrueGrid User's Manual*, 1995]

The FEA codes used for the 3D modeling were NIKE3D and LS-NIKE3D. NIKE3D is a nonlinear, implicit, 3D finite element code for solid and structural mechanics. NIKE3D uses beam, shell, and hexahedral elements and a variety of elastic and inelastic material models. It has contact-impact algorithms that permit gaps, frictional sliding, and mesh discontinuities along material interfaces. NIKE3D was originally developed by John Hallquist of the Methods Development Group at LLNL, with continued development by Bradley Maker and Robert Ferencz. [Maker, 1991]

LS-NIKE3D is an implicit, finite-deformation, finite element code for analyzing the static and dynamic response of three dimensional solids. LS-NIKE3D was developed by Livermore Software Technology Corporation (LSTC) from the NIKE3D code developed at LLNL. Major developments made in the contact algorithms and the linear equation solving technology have made LS-NIKE3D robust and efficient. [*LS-NIKE3D User's Manual*, 1996]

The post processor used to view the results generated by the 3D FEA code was LS-TAURUS. LS-TAURUS is a highly interactive post-processor developed by LSTC to display results of LLNL and LSTC families of 3D FEA codes. It originated from LLNL post-processors developed by John O. Hallquist. [*LS-TAURUS User's Manual*, 1995]

3.3 FATIGUE

Fatigue is the process responsible for premature failure or damage of components subjected to repeated loading [Bannantine and Comer, 1990]. Fatigue is considered low cycle if the number of load cycles to failure is less than 1000 cycles, and high cycle if the number of load cycles to failure is more than 1000 cycles. Fatigue is often divided into two phases; crack initiation and crack propagation. Crack initiation is the phase where a crack is formed, usually around an inclusion or other defect. Crack propagation occurs when the crack increases in length with subsequent load cycles. The boundary between the two phases is often very difficult to determine.

Three general methods of fatigue analysis are used in analysis and design. They are strain-life, stress-life, and linear-elastic fracture mechanics. Each method has both strengths and weaknesses and each may be more appropriate for different classes of problems. Knowledge about the material, loading, geometry, whether the fatigue is low or high cycle, and whether the phase of interest is initiation and/or propagation is helpful in determining which method is most appropriate.

3.3.1 STRAIN-LIFE FATIGUE ANALYSIS

The strain-life method uses the true strain to predict the number of cycles to failure. When components are under high load and/or have critical locations (notches), the stress-strain relationship is no longer linearly related. In these situations, the plastic strain becomes a significant part of the deformation. Since the primary mechanism in fatigue is plastic deformation, an elastic model is not appropriate. The strain-life method uses the level of deformation explicitly, and it is more appropriate for cases with high plastic deformation. These types of cases fall into the low cycle fatigue category.

The strain-life method is used by comparing the true strain range to a strain vs. fatigue life curve. One weakness of this method is that finding true strain in areas of discontinuities can be very difficult. More experimental data is needed to account for surface finish, surface treatment, loading, and other modifying parameters.

3.3.2 STRESS-LIFE FATIGUE ANALYSIS

The stress-life method uses the alternating stress amplitude to predict the number of cycles to failure. This method is based on comparing the stress amplitude to a stress vs. fatigue life curve, S-N diagram. These curves are based on empirical formulas derived from experimental data. The stress-life method is generally only used for high cycle fatigue because under low cycle fatigue, the stress-strain relationship becomes nonlinear.

For many metals (including steel) there exists a region of infinite life, where fatigue problems will not develop if the stress amplitude is below a threshold value. This threshold value is called the endurance limit (S_e) [Shigley and Mischke, 1989]. In many materials, the endurance limit has been related to the ultimate tensile strength (S_{UT}) through experimental testing. The ideal endurance limit (S_e') for steels with a ultimate tensile strength less than 200 ksi is roughly $0.5 \cdot S_{UT}$ [Shigley and Mischke, 1989]. The ideal endurance limit is calculated in a laboratory where the conditions of the experiment and the specimen are carefully controlled. The ideal endurance limit is then related to the actual endurance limit by applying factors that account for differences in surface finish, surface treatments, size, temperature, loading, and other environment factors [Bannantine and Comer, 1990].

The S-N diagram is a log scale plot of the fully reversed stress amplitude vs. the number of stress cycles to failure. For steel, the S-N diagram is generally drawn by connecting a line from the fatigue strength at 10^3 cycles to the endurance limit (S_e) at 10^6 cycles. The fatigue strength at 10^3 is only slightly less than the S_{UT} and is taken to be $0.9 \cdot S_{UT}$. [Shigley and Mischke, 1989]

For the cases where the stress mean is not zero, an equivalent stress amplitude (S) must be calculated from the mean stress (σ_m) and the stress amplitude (σ_a). There are two relationships that tend to bracket the test data. They are the Goodman and Gerber relationships. The equations are shown below. The Goodman relationship is the more conservative of the two and is often used for that reason. [Bannantine and Comer, 1990]

$$\text{Goodman Relationship} \quad S = \frac{\sigma_a}{1 - \frac{\sigma_m}{S_{UT}}} \quad (3-1)$$

$$\text{Gerber Relationship} \quad S = \frac{\sigma_a}{1 - \left(\frac{\sigma_m}{S_{UT}}\right)^2} \quad (3-2)$$

The endurance limit is based on a constant amplitude alternating stress. There are many instances where the stress amplitude is variable. In these cases, a method for calculating cumulative damage is used to find an effective alternating stress. A root mean cubed method is often used to estimate cumulative damage [Moses, et al, 1987]. The individual stress range values are first cubed, an average is taken, and then the cube root of the average is determined. The result is a effective stress range value that is larger than the value obtained from the arithmetic average because cubing the stress range values increases the emphasis on the large values in the distribution. If the alternating stress is not fully reversed, an equivalent stress amplitude is then calculated using either the Goodman or Gerber relationship.

Even though the effective stress amplitude may be less than the fatigue limit, many amplitudes may still fall above the fatigue limit. This typically results in a finite life. Distributions with as low as one stress amplitude in thousand above the fatigue limit have still been found to exhibit a finite life [Fisher, et al, 1983].

One method of calculating the finite life for variable amplitude alternating stress is to extend the S-N curve beyond the constant amplitude fatigue limit [Moses, et al, 1987]. The slope of this extension can be adjusted to reflect the distribution of cycles above the constant amplitude fatigue limit.

The stress-life method is completely empirical in nature and is limited to cases of high cycle fatigue only. It has, however, been used for many years and there is a considerable amount of experimental data that has been used to derive empirical solutions.

3.3.3 LINEAR-ELASTIC FRACTURE MECHANICS

Linear-elastic fracture mechanics (LEFM) is an analytical method that relates the stress at a crack tip to the nominal stress field around the crack. LEFM began with Griffith's work in the 1920's. Griffith proposed that for brittle materials a crack will propagate if the total energy of the system is reduced by the propagation. In the 1940's, progress continued with Irwin's work; a theory for ductile materials was added. Irwin reported that the energy applied to plastic deformation must be included by adding it to the surface energy associated with the new crack surface. In the 1950's, Irwin also developed equations for the local stresses near the crack tip. [Bannantine and Comer, 1990]

There are three modes describing crack displacement: Mode I; opening or tensile mode, Mode II; sliding or in-plane shear, and Mode III; tearing or anti-plane shear. Figure 3.1 shows a schematic representation of each of these three modes. For most structures Mode I is the dominate condition.

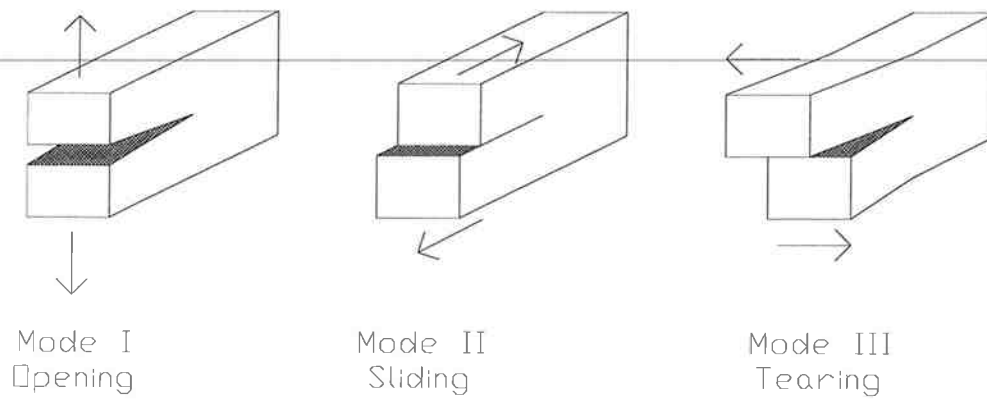


Figure 3.1 Three modes of crack displacement.

With the existence of a crack, there is an infinite stress concentration at the crack tip. The stress intensity factor, K , allows the singularity to be dealt with in terms of strain energy. The stress intensity factor describes the entire stress state around the crack tip. K is a function of the nominal stress, crack length, and geometric factors. The stress intensity factor is described by [Fisher, et al, 1989] as

$$K = F_e \cdot F_s \cdot F_w \cdot F_g \cdot \sigma \cdot \sqrt{\pi \cdot a} \quad (3-3)$$

where a is the crack length for an edge crack and half the crack length for an internal crack, σ is the nominal tensile stress normal to the crack plane, F_e is a factor for crack shape, F_s is a factor to account for surface cracks, F_w is a factor for a specimen with finite width, and F_g is a factor for non-uniform nominal stress.

If the stress intensity at the crack tip reaches a critical value the crack will begin unstable propagation. This critical stress intensity is called the fracture toughness (K_C). The fracture toughness can be used to calculate the critical crack length at which unstable propagation will occur. For Mode I crack displacement with plane strain conditions existing at the crack tip, the fracture toughness is denoted by K_{IC} . K_{IC} values are obtained by using the standard ASTM test method, E-399-83 [Barsom and Rolfe, 1987].

There are three regions of the fatigue crack growth. Region I includes the initiation stage where the crack growth rate is small and threshold effects are important. Region II is a region of consistent and predictable crack growth rate. Region III is a region of rapid and unstable crack growth rate. Generally, region III does not contribute significantly to the fatigue life and is ignored [Bannantine and Comer, 1990].

The stress intensity can be related to the fatigue crack growth rate, (da/dN) . When the stress field around a crack is alternating this produces an analogous alternating stress intensity factor (ΔK). ΔK is calculated the same as K except that σ is replaced by $\Delta\sigma$. In Region II the slope of the log da/dN versus the log ΔK curve is linear, and da/dN and ΔK are related by the Paris equation from [Shigley and Mischke, 1989]

$$\frac{da}{dN} = C \cdot [\Delta K(a)]^M \quad (3-4)$$

where da/dN is the crack growth rate, ΔK is the alternating stress intensity factor, N is the number of cycles, and C and M are empirical constants of the material. The fatigue life is determined by evaluating the integral

$$N = \int_{a_i}^{a_f} \frac{1}{C \cdot [\Delta K(a)]^M} da \quad (3-5)$$

where a_i is the initial crack size, a_f is the final crack size. The final crack size is usually set as the critical crack size. The initial crack size is often set as the size of largest defect that is expected to be present. The largest defect size is often difficult to determine. The initial crack size is very important because, when the crack length is small, the crack growth rate is also very small.

4.0 LOADING ANALYSIS

This chapter describes two analysis methods used to calculate the distribution of live truck loads on the stringers. The first method, stringer loading analysis is a linear-elastic analysis hand calculation. The second method, the global FEA model, was performed using the finite element method. A model validation analysis of the global FEA model is also discussed. The live loading results of the two analyses are also presented in section 4.3.

For both analysis methods, the suggested standard fatigue truck, outlined in the NCHRP Report 299 [Moses, et al, 1987], is used for model loading. Figure 4.1 shows a diagram of the standard fatigue truck. This truck was developed to represent the variety of different types and weights of

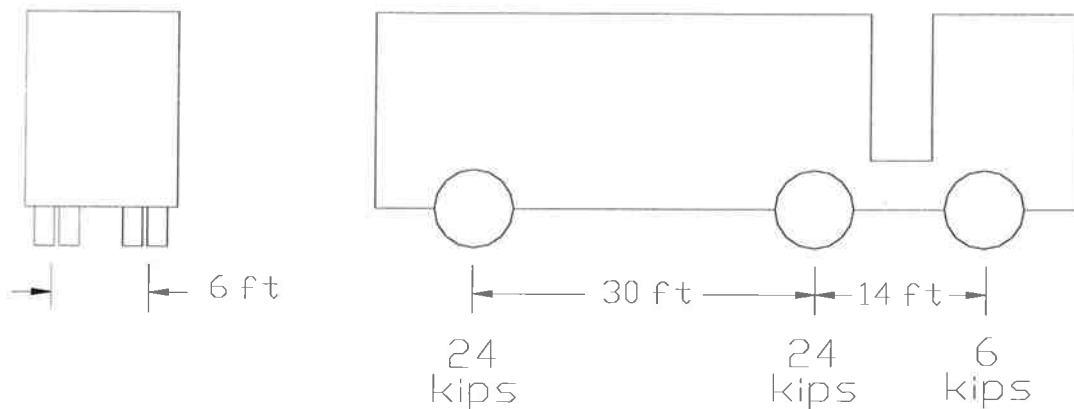


Figure 4.1 Suggested standard fatigue truck outlined in the NCHRP Report 299.

trucks in actual traffic. It consists of two rear axles of 24 kip each and a front axle of 6 kip. The rear axles are spaced 30 feet while the front and the first rear axle are spaced 14 feet. The width of each axle is 6 feet.

4.1 STRINGER LOADING ANALYSIS

The distribution of the truck loads through the deck on the stringers is important in determining the loading on the clip angle. The loads on each stringer were calculated with one rear axle of the fatigue truck positioned longitudinally in the center of a panel over the mid length of the stringers. Laterally, the axle was centered in the slow lane of traffic. For both the north and southbound structures, three stringers are assumed to carry the entire weight of the axle. Those

stringers are the middle stringer, the 2nd from the middle stringer, and the 3rd from the middle stringer in the slow lane. Figure 4.2 shows a diagram of the location of the three stringers.

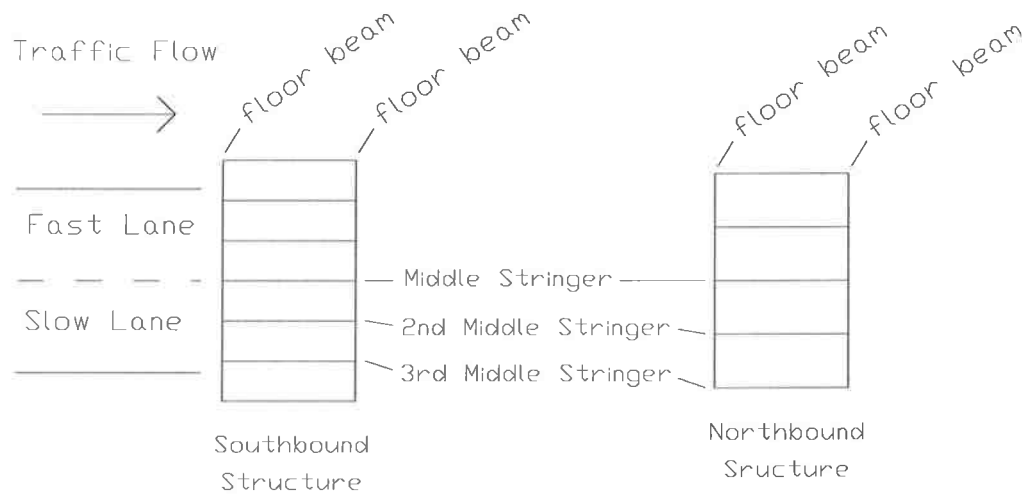


Figure 4.2 Top view diagram of the three stringers that are assumed to carry the axle load in the stringer loading analysis.

Each section of the deck between the three stringers was analyzed as an independent beam using beam tables from [Shigley and Mischke, 1989]. The stringer loads were calculated as the reaction forces at the ends of the beams. Figure 4.3 shows a diagram of the loading and boundary conditions. The stringer loads for both the north and southbound structures can be found in results section. For details of the analysis see Appendix A.

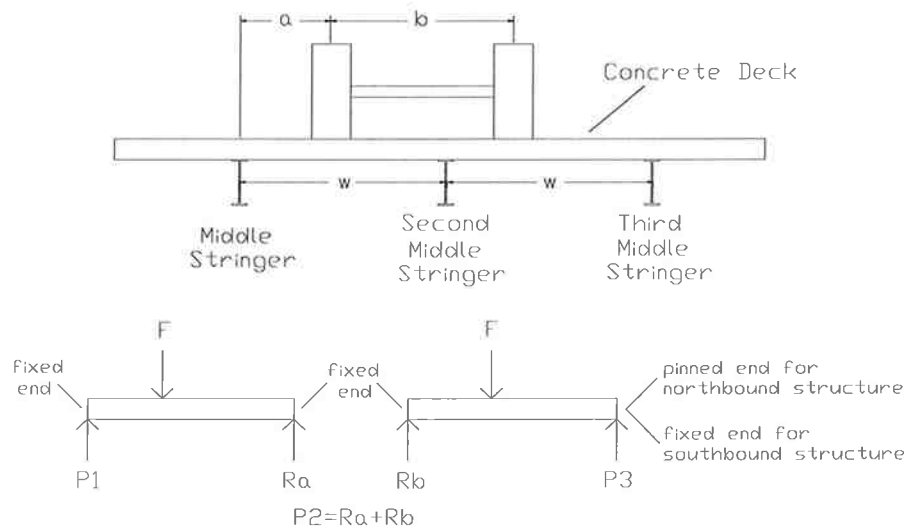


Figure 4.3 Diagram of the loading and boundary conditions used in the stringer loading analysis.

4.2 GLOBAL FEA MODEL

Finite element models for both the north and southbound structures were developed to determine the distribution of loads on the stringers. The floor beams, stringers, clip angles, and the reinforced concrete deck of one panel are included in the model. 3D beam elements were used to model the floor beams and stringers. Orthotropic plate elements were used to model the reinforced concrete deck. The properties of the orthotropic plate elements were determined by performing an analysis of the reinforced concrete deck. Discussion of this analysis can be found in the following section.

Beam elements with a length of 0.1 inches were used to model the boundary conditions created by the clip angles and floor beams. Because the boundary beam elements modeled the compliance of the floor beams, the rotation of the floor beams were fixed. The area moment of inertia of the boundary beam elements was set so that the end rotation at the end of the stringer beam elements matched the rotation of the clip angle from the clip angle deflection analysis. When results became available from the 3D FEA model, the properties of the boundary beam elements were adjusted. Two boundary beam elements were developed from the results of the 3D FEA model. One modeled the connection details in the interior of the span, and the other modeled the connection details at the end of the span.

Models of both an end panel and an interior panel were developed for each of the north and southbound structures. One axle of the standard fatigue truck was used to load the models. The distribution of loads on the stringers were the primary interest. It was observed that the properties of the boundary beam elements, the area moment of inertia of the stringers, and the longitudinal position of the axle did not play a significant role in the loading of the stringers. Individual loading on the stringers is strongly dependent upon both the lateral position and the width of the load axle. This indicates that detailed knowledge about the position of the stringers in relationship to the lanes of traffic is important. It also demonstrates the necessity of having a fatigue truck that accurately represents the population of trucks.

The stringer loads calculated from the global FEA model can be found in section 4.3. The COSMOS command files can be found in Appendix B.

4.2.1 REINFORCED CONCRETE DECK ANALYSIS

A six inch thick reinforced concrete deck is used to transmit the traffic load to the stringers and floor beams. An analysis was performed to quantify the equivalent stiffness of the concrete deck. During construction rebar was inserted in both the longitudinal and transverse directions to give the deck the tensile strength it needs to support the traffic loads. The position and amount of rebar added in each direction is different. For this reason, it was necessary to quantify the reinforced concrete deck stiffness properties in each direction separately.

The orthotropic properties of the deck were calculated by following the procedure outlined in *Reinforced Concrete Design* [Everard and Tanner, 1966]. The properties in each direction were calculated independently. A beam of unit width, with the top portion of the beam associated with compression and the bottom portion associated with tension, was used to model the deck. The reinforcing steel in the top region of the deck was placed in the compression portion of the deck and the steel in the bottom portion of the deck was placed in the tension portion. One exception was made however. In the transverse direction sections of the rebar change depth. The rebar was installed so that it was always in the portion of the deck that would be in tension. It is in the upper region of the deck over the stringers and is in the lower region between the stringers. For this reason, it was placed in the tension portion of the model.

The assumption that the concrete could only contribute strength in compression was used in the analysis. This created a beam model that had concrete and steel on the compression side and steel alone on the tension side. Area moments of inertia per unit width were calculated for both the transverse and longitudinal directions. These area moments of inertia were then used to find equivalent moduli of elasticity for a six inch thick uniform deck. The resulting moduli of elasticity for the transverse and longitudinal directions were 1300 ksi and 546 ksi, respectively. See Appendix C for details of the analysis.

4.2.2 Model Validation

Field testing was performed on the Winchester Bridge by the Oregon Department of Transportation to quantify the live loading and to assist in validating the analysis. Five strain gages were installed on the top of the bottom flanges at mid span of three stringers and two floor beams of one span of the northbound structure. The uniaxial, 350 ohm strain gages had a gage length of 0.25 inches and were used in a three wire quarter bridge configuration. Samples were taken at a rate of 60 Hz with a 30 Hz low pass filter. The sensitivity of the strain measurements is +/- 10 microstrain.

Strain gauges were installed on the first and second floor beams of the first span. Two stringers from the first panel and one stringer from the second panel were installed with strain gages. Figure 4.4 shows the stringers and floor beams that were gauged.

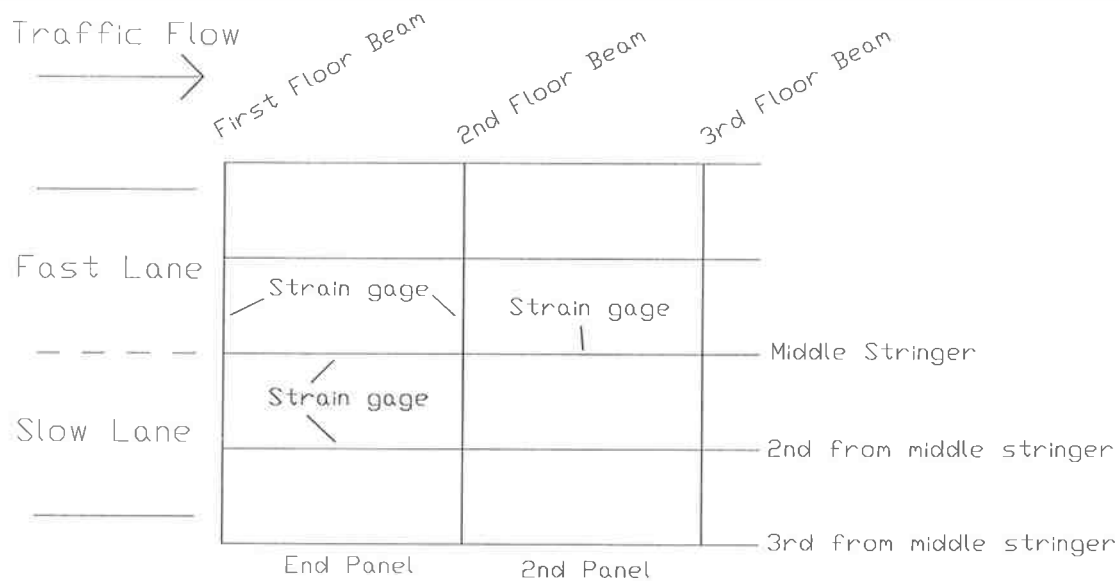


Figure 4.4 Three stringers and two floor beams on the northbound structure of the Winchester Bridge that had strain gauges installed.

In the first panel, the middle stringer and the second from middle stringer in the slow lane had strain gages installed. In the second panel, the second from the middle stringer in the slow lane had a strain gage installed.

Data were taken under normal traffic flow with both lanes open and under a known truck weight with the slow lane closed. Figure 4.5 shows the comparison of the measured stress ranges in the stringer to those calculated from the global FEA model for the known truck weight. Stress ranges from the known truck weight are compared to the stress ranges calculated in the global FEA model loaded with the known truck weight. Figure 4.6 shows the comparison of the measured stress ranges in the stringers to those calculated from the global FEA model for random truck traffic. The cubed-root mean of the measured stress ranges for the random truck traffic are compared to the stress ranges calculated in the global FEA model loaded with the standard fatigue truck.

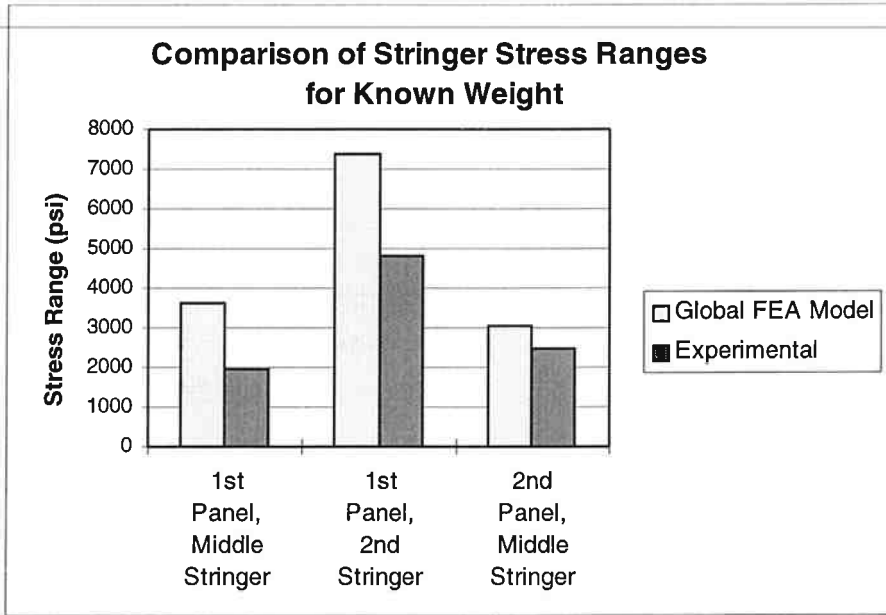


Figure 4.5 Graph of the stringer stress ranges from the global FEA model and those measured experimentally, loaded with a known truck weight.

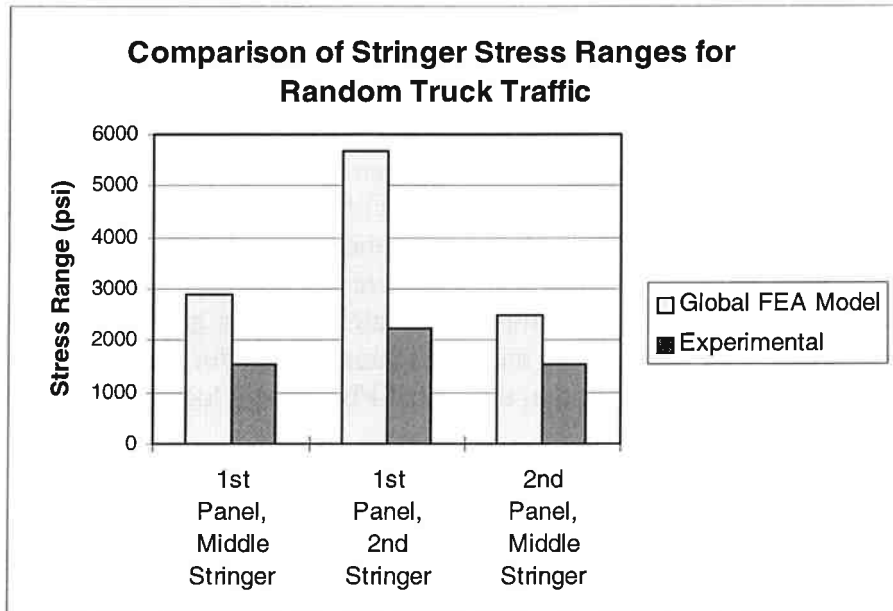


Figure 4.6 Graph of the stringer stress ranges from the global FEA model and those measured experimentally, under random traffic loading.

The measured stresses are much lower than those calculated from the global FEA model. This indicates that the composite interaction between the deck and the stringers, an interaction that is not modeled in the global FEA model, is important. If shear loads are transferred between the deck and the stringers, the neutral axis is shifted upward and the area moment of inertia is increased. The effect is that the section modulus for the stringer is increased, resulting in a lower stress range.

The composite interaction between the deck and the stringers could be quantified if strain data were available for both the top and bottom flanges. The ratio of strain ranges could be used to calculate the position of the neutral axis, and the known load and the strain range of the bottom flange could be used to calculate the section modulus. The effective area moment of inertia could then be calculated from the new position of the neutral axis and the new section modulus.

Another possible reason, for the difference in calculated and measured stress ranges, is that the actual reinforced concrete deck is stiffer than was calculated. Assuming that concrete only contributes strength in compression is a conservative assumption. A stiffer deck would increase the distribution of the axle load to other stringers.

4.3 RESULTS

Two stringers in each panel of the northbound structure are loaded significantly. A significant load was considered to be one that was greater than 3000 lb. They are the middle stringer and the 2nd from middle stringer on the slow lane side. Three stringers in each panel of the southbound structure are loaded significantly. They are the middle stringer, 2nd from the middle stringer, and the 3rd from middle stringer on the slow lane side. Figure 4.7 is a graph of the stringer loads for the northbound structure. Figure 4.8 is a graph of the stringer loads for the southbound structure.

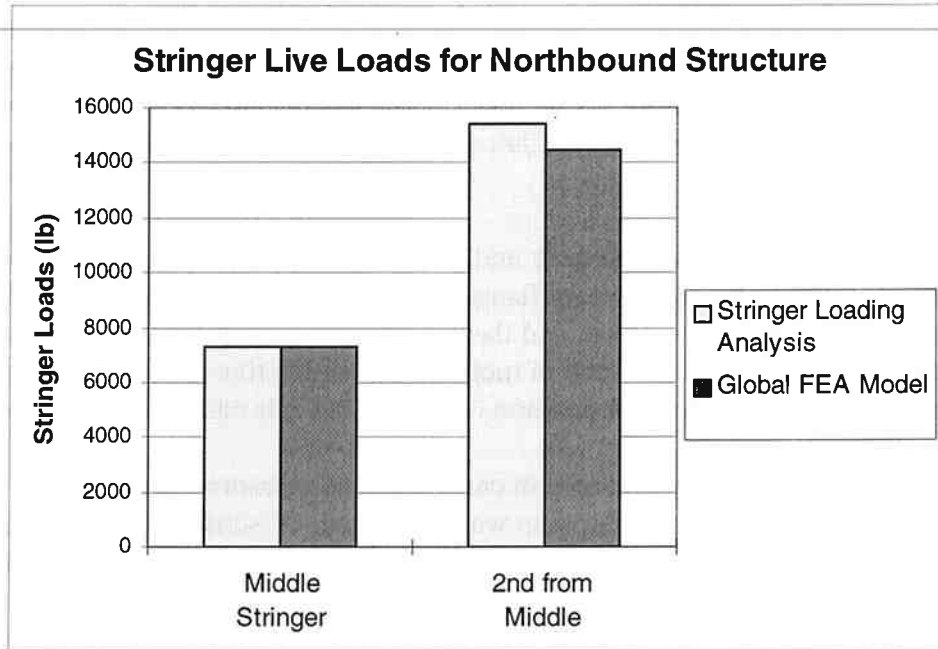


Figure 4.7 Graph of the stringer loads for the northbound structure for both the stringer loading analysis and the global FEA model.

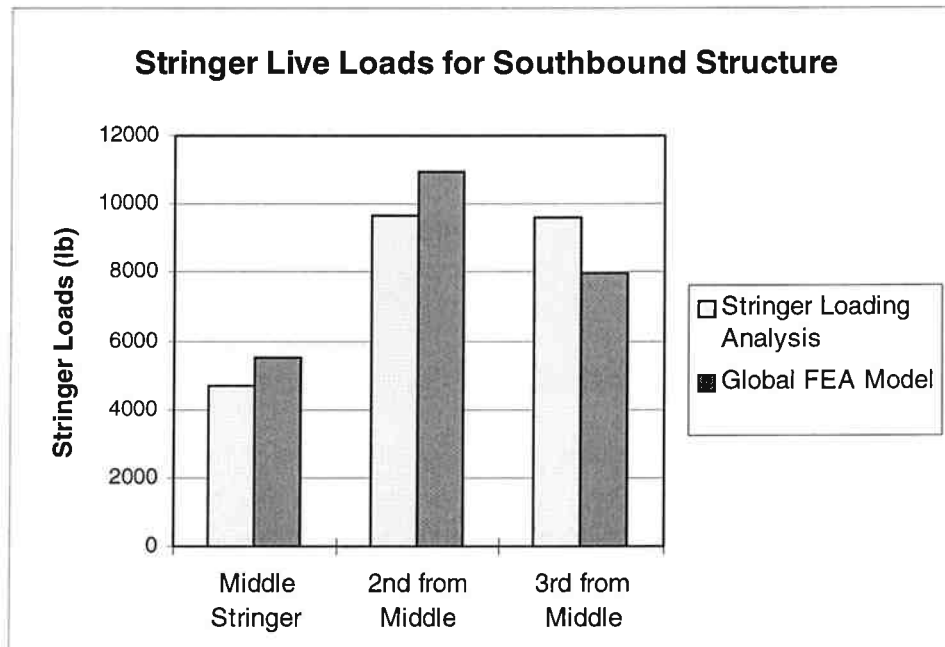


Figure 4.8 Graph of the stringer loads for the southbound structure for both the stringer loading analysis and the global FEA model.

It can be observed that the results between the two methods are in reasonable agreement. This is interesting because for the stringer loading analysis it was assumed that the entire axle load is carried by three stringers. These results suggest that this assumption is correct for a six inch reinforced concrete deck.

Changes in the deck stiffness were investigated by increasing the deck thickness in the global FEA model. Figure 4.9 shows the loads on the 2nd from middle stringer vs. the deck thickness of both the north and southbound structures.

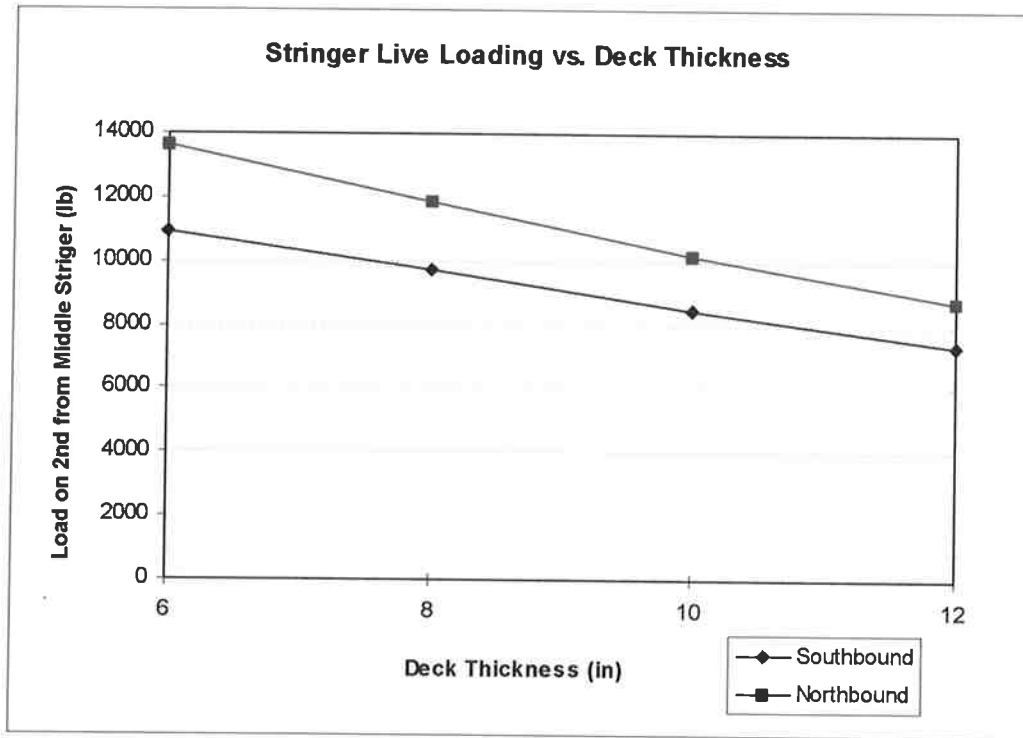


Figure 4.9 Graph of the load on the 2nd from middle stringer vs. the deck thickness from the global FEA model.

It can be observed that as the deck thickness is increased, the axle load is distributed to other stringers. This is an important discovery since the reinforced concrete deck thickness is different on other structures. Information about the effect that the deck thickness has on the loading on the stringers can easily be used to estimate the stringer loads in other bridge structures. The assumption that the effective moduli of elasticity of other bridge decks are the same as the moduli of that calculated for the Winchester Bridge would have to be accounted for in any subsequent deck stiffness analysis.

5.0 DEFLECTION AND STRESS ANALYSIS

The clip angle creates a unique boundary condition for the stringer. The compliance of this connection is somewhere between that of an ideal fixed and an ideal pinned connection. When the stringer is loaded, there is a resulting end reaction moment, M_o between the clip angle and stringer. The clip angle deflection, δ_m , the end stringer rotation, θ_{ST} , and the level of stress in the clip angle are dependent upon M_o . Since only live loading was considered, the maximum level of stress in the clip angle translates to a stress range. The three analysis techniques used to investigate these relationships are discussed in the following sections.

5.1 CLIP ANGLE DEFLECTION AND STRESS ANALYSIS

To determine the end moment, M_o , the stringer was modeled as a pinned beam with the moments, M_o , acting on the ends and the stringer load, P , acting in the middle. Figure 5.1 shows the model of the stringer.

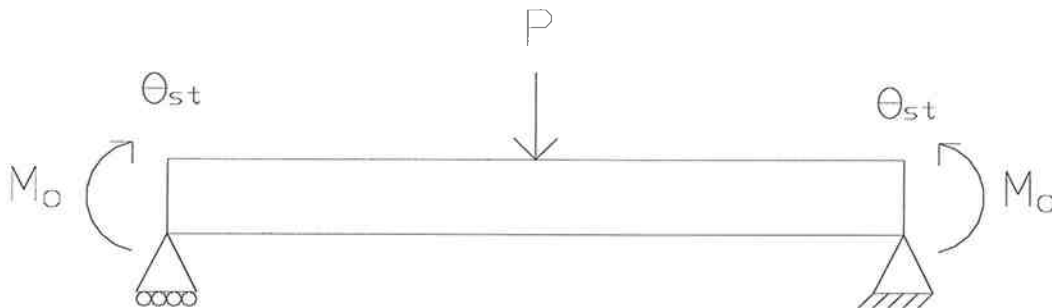


Figure 5.1 Stringer model, illustrating loading and boundary conditions.

Using beam tables from [Gere and Timshenko, 1990], the end rotation of the stringer, θ_{ST} , is written as

$$\theta_{ST} = \frac{P \cdot L^2}{16 \cdot E \cdot I} - \frac{M_o \cdot L}{2 \cdot E \cdot I} \quad (5-1)$$

where L is the length of the stringer, I is the area moment of inertia of the stringer, and E is the Young's modulus of the stringer.

An Euler beam analysis was performed to determine the deflection of the clip angle, δ_m , as a function of the end moment, M_o . To find this relationship, the top of the floor beam leg of the clip angle was modeled as a cantilever beam with a force per unit length, F_R and a moment per unit length, M_R acting on the end. Figure 5.2 shows a diagram of the cantilever beam model of the clip angle.

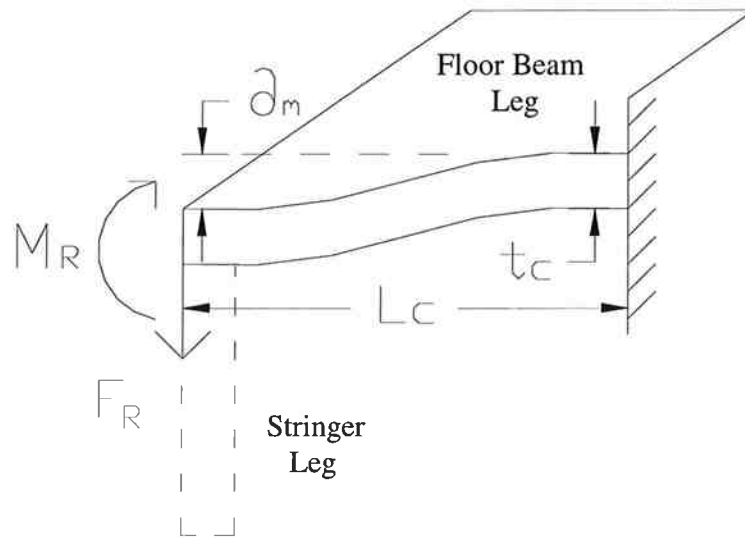


Figure 5.2 Top of the floor beam leg of the clip angle modeled as a cantilever beam.

F_R is a result of the moment, M_o , and is calculated by assuming that center of rotation of the clip angle is at the bottom. Figure 5.3 is a diagram showing how F_R is related to M_o .

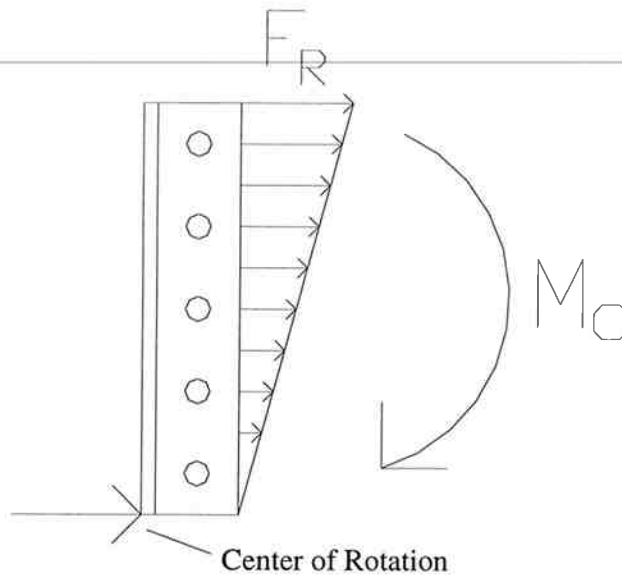


Figure 5.3 Diagram of clip angle showing the center of rotation and the relationship of F_R and M_o .

F_R is written as a function of M_o as

$$F_R = \frac{3 \cdot M_o}{2 \cdot h^2} \quad (5-2)$$

where h is the height of the clip angle.

The stringer leg of clip angle restricts the rotation at the corner of the clip angle. For this reason, the assumption was made that rotation at the end of the beam model of the clip angle is zero. M_R is the moment at the corner of the clip angle restricting the rotation of the corner of the clip angle. By setting the end rotation equal to zero, M_R was found as a function of F_R ,

$$M_R = \frac{F_R \cdot L_C}{2} \quad (5-3)$$

where L_C is the length of the clip angle beam model. The deflection, δ_m of the clip angle was then found as a function of the end moment, M_o . The clip angle rotation is calculated (by small

angle theorem) as the deflection divided by the height of the clip angle. The expression for the clip angle rotation is

$$\theta_{c1} = \frac{\delta_m}{h} = C_R \cdot M_o \quad (5-4)$$

$$C_R = \frac{3 \cdot L_c^3}{2 \cdot E \cdot t_c^3 \cdot h^3} \quad (5-5)$$

where C_R is the clip angle rotation constant, L_c length of the beam, E is the Young's modulus, t_c is the clip angle thickness, and h is the height of the clip angle.

Due to physical constraints, the rotation of the clip angle and the end rotation of the stringer must be equal. The moment was found as a function of both stringer and clip angle parameters and is shown as

$$M_o = \frac{\frac{P \cdot L^2}{16 \cdot E \cdot I}}{C_R + \frac{L}{2 \cdot E \cdot I}} \quad (5-6)$$

where P is the load on the stringer, L is the length of the stringer, I is the area moment of inertia of the stringer, E is the Young's modulus of the stringer, and C_R is the clip angle rotation constant. This equation is important because values of C_R that are determined from the results of the 3D FEA model can also be inserted into the equation above to calculate M_o . See Appendix D for details of the derivation.

The moment in the leg of the clip angle is highest at the corner of the clip angle where the stringer leg and floor beam leg of the clip angle come together. However, the maximum stress range is not located at the corner because at the corner the clip angle thickness is increased due to the corner fillet. See Appendix E for details of the calculation of the maximum stress in the clip angle. The clip angle deflections and stress ranges can be found in the results section.

5.2 2D FEA MODEL

A 2D FEA model of the top section of the clip angle was developed to determine the deflections and stress ranges in the clip angles. Plain stress plate elements of unit depth were used to build the model. Figure 5.4 shows the boundary conditions and loading of the 2D FEA model.

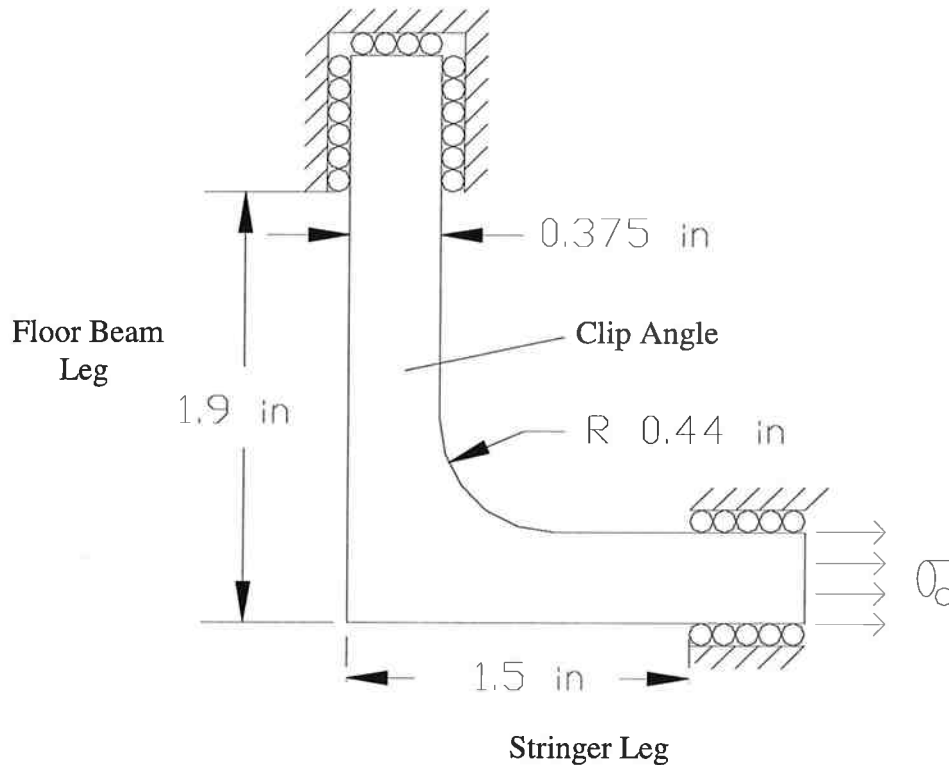


Figure 5.4 2D FEA model of the top of the clip angle illustrating size dimensions, boundary conditions, and loading.

Fixed boundary conditions were used to model the riveted connections of the clip angle to the floor beam and the stringer. The assumption was made that the riveted connections between the clip angle and the floor beam and stringer were located at the top of the clip angle, when they were actually located 1.5 inches down from the top. This simplification results in a reduction of compliance but was necessary because of the nature of the 2D model. A uniform pressure load, σ_0 , was applied to the stringer leg of the clip angle to model the axial loading at the top of the clip angle from the stringer. This pressure is a result of the moment, M_0 , at the end of the stringer and is found by dividing the expression for the force per unit length, F_R , by the clip angle thickness. The expression for σ_0 is

$$\sigma_o = \frac{F_R}{t_c} = \frac{3 \cdot M_o}{2 \cdot t_c \cdot h^2} \quad (5-7)$$

where t_c is the thickness of the clip angle, h is the height of the clip angle, and M_o is the moment transferred to the clip angle from the stringer.

Stress ranges and deflections for the different clip angles can be found in the section 5.4. The MAZE command files and further details of the analysis can be found in Appendix F.

5.3 3D FEA MODEL

A 3D FEA model of a clip angle, a stringer, and a section of floor beam was developed to accurately determine the deflection and the stress in the clip angle. The clip angle, stringer, and floor beam were meshed as separate parts with hexahedral brick elements.

Symmetry planes were used to decrease the number of elements in the model. The model was divided into four quadrants by placing planes of symmetry both longitudinally down the center of the stringer and laterally at the mid point of the stringer.

Slide-surfaces were used as interfaces between the three parts. The contact algorithms allow non-linearity, such as gaps and frictional sliding to be modeled.

The riveted connections between the stringer, clip angle, and floor beam were important parts of the model. The rivets used to connect the stringer and clip angle were meshed as part of the stringer. The rivets used to connect the floor beam and the clip angle were meshed as part of the floor beam. Slide surfaces were used between the rivets and the clip angle. A pre-load of 25 kip was applied to the rivets to approximate the as installed rivet pre-load.

The majority of steel deck truss span bridges under the responsibility of ODOT contain connection details that are made of $3 \frac{1}{2} \times 4 \times \frac{3}{8}$ inch angles as in the Winchester Bridge and $3 \frac{1}{2} \times 4 \times \frac{1}{2}$ inch angles. For this reason both $\frac{3}{8}$ inch and $\frac{1}{2}$ inch thick clip angles were modeled and analyzed.

Several factors were investigated to determine their effect on the deflection and stress range of the clip angle. They are discussed in the following sections.

5.3.1 ELEMENT DENSITY

Element density was the first factor investigated. Generally, the accuracy of a finite element model increases as the number of elements increases until the mesh is sufficiently fine and

further mesh refinement does not yield a significant increase in accuracy. The analysis time is also increased as the number of elements is increased. It follows that it is desirable to use the minimum number of elements that still produce accurate results.

The effect that the element density had on the model was explored by changing the number of elements across the thickness of the clip angle. It was discovered that the deflections of the clip angle and the end rotation of the stringer did not depend significantly on the element density. The stress range did, however, depend on the density.

When the number of elements across the thickness of the $\frac{3}{8}$ inch thick clip angle was increased from four to five, the maximum stress range increased by 8%. When the number of elements was increased from five to six, the maximum stress range only increased by 4%. It was deemed that, for the $\frac{3}{8}$ inch thick clip angle, six element across the thickness was adequate.

When the number of elements across the thickness of the $\frac{1}{2}$ inch thick clip angle was increased from five to six, the maximum stress range increased by 17%. When the number of elements was increased from six to seven, the maximum stress range only increased by 5%. It was deemed that, for the $\frac{1}{2}$ inch thick clip angle, seven elements across the thickness was adequate.

5.3.2 BOUNDARY CONDITIONS

The boundary conditions for the floor beam mesh made a significant difference in the deflection and stress of the clip angle. Floor beams at the end of the span with stringers connected to only one side have different boundary conditions than floor beams in the interior of the span with stringers connected to both sides. Two sets of boundary conditions were investigated for the floor beam mesh. They were the fixed rotation model and the fixed top flange model.

The interior floor beams were modeled using the fixed rotation model. In this model, the floor beams rotation is fixed throughout the length of the mesh. The assumption was made that rotation of the interior floor beams is zero because their rotation is restricted by stringers attached to both sides.

The floor beams at the end of the span were model using the fixed top flange model. In this model, the ends of the floor beam and the top flange of the floor beam were fixed. The top flange of the floor beam was fixed to model the restriction that the reinforced concrete deck applies to the floor beam.

5.3.3 RIVET PRE-LOAD AND FRICTION

Rivet pre-load and friction were used to increase the accuracy of the riveted connection. The rivet pre-load is applied by lowering the temperature of the rivets, causing them to thermally contract. This is done in a time step before the stringer is loaded. Friction was applied by changing the coefficient of friction from 0.0 to 0.5. The static and sliding coefficients of friction for mild steel on mild steel is 0.74 and 0.57 respectively [Marks, 1996].

When the friction and rivet pre-load are applied to the model, the connection between the stringer and clip angle was changed. The rivet pre-load produces high normal forces at the interfaces between the stringer, clip angle, floor beam, and rivets. The frictional forces increase the stiffness of the connection between the stringer and the clip angle reducing the end rotation of the stringer and increasing the flexural moment transmitted to the clip angle.

The pre-load and friction also change the stress flow through the clip angle. When there is no pre-load and friction, the load from the rivet is forced to go around the rivet holes. When pre-load and friction are applied, the load is transmitted across the rivet hole by the frictional forces between the rivet, clip angle, and stringer. This results in a more localized stress concentration in the clip angle. The location of the stress concentrations will be discussed in section 5.4.

5.3.4 CLIP ANGLE THICKNESS

The clip angle thickness was another factor that was investigated. Models were created for $\frac{3}{8}$ and $\frac{1}{2}$ inch thick clip angles. For the same loading and floor beam boundary condition of fixed rotation, the deflection of the $\frac{1}{2}$ inch clip angle was 28% lower than the $\frac{3}{8}$ inch clip angle, and the maximum stress range decreased by 8%. The rotation of the end of the stringer with the $\frac{1}{2}$ inch clip angle decreased by about 12%.

The stress ranges for the different clip angles are presented in the section 5.4. The stress ranges are from models that included friction and pre-load. A TrueGrid command file and additional results can be found in Appendix G.

5.4 RESULTS

Figures 5.5 and 5.6 are exaggerated deflection plots for interior panel clip angles from the 2D FEA model and 3D FEA model, respectively.

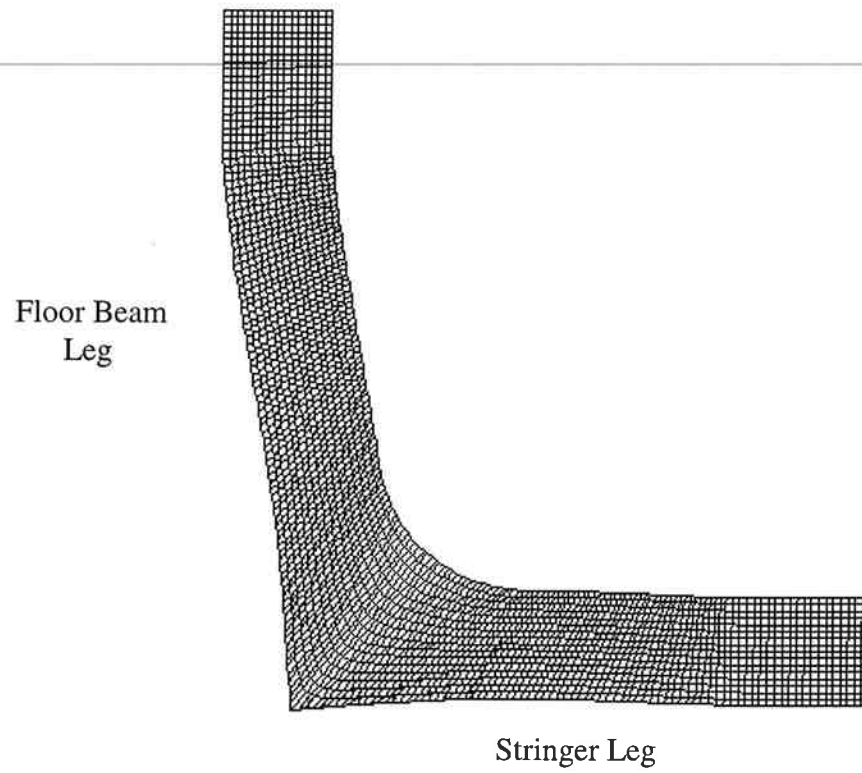


Figure 5.5 Exaggerated deflection plot from the 2D FEA model of an interior panel clip angle.

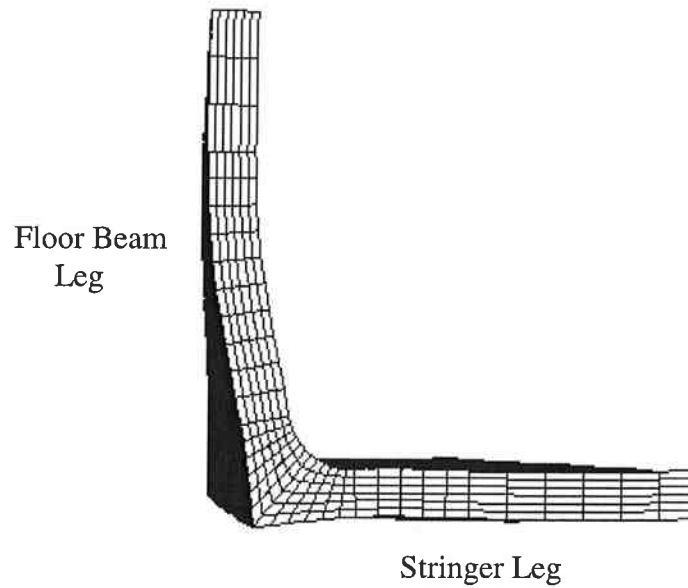


Figure 5.6 Exaggerated deflection plot from the 3D FEA model of an interior panel clip angle.

The shape of the two plots appear very similar; they both show that there is rotation at the corner. This indicates that the assumption made in the clip angle deflection analysis, that the corner of the clip angle is zero, is incorrect.

The results from the clip angle deflection analysis and the 2D FEA model represent clip angles located in the interior panels only. Table 5.1 shows the deflections calculated from each analysis method for the interior panel clip angles.

Table 5.1: Comparison of Interior Panel Clip Angle Deflections (in.) from Each Analysis Method.

Analysis Method	Northbound		Southbound		
	Middle	2nd	Middle	2nd	3rd
Clip Angle Deflection Analysis	0.0019	0.0037	0.0014	0.0029	0.0021
2D FEA Model	0.0039	0.0078	0.0031	0.0061	0.0044
3D FEA Model	0.0033	0.0066	0.0025	0.0050	0.0036

The clip angle deflection analysis predicts the lowest clip angle deflection. The reason that the clip angle deflections were so low, compared to the other two analyses was the assumption of zero rotation at the clip angle corner was incorrect. Both the 2D FEA and 3D FEA deflection plots show that the rotation was restricted but not zero.

The deflection predicted from the 3D FEA model was about 16% smaller than the deflection predicted from the 2D FEA model. The reason for this is that in the 3D FEA model there was relative movement between the stringer and clip angle. In the 2D FEA model, the simplifying assumption was made that the rotation of the clip angle and rotation of the end of the stringer is the same. The relative movement adds to the compliance of the connection, reducing the flexural moment applied to the clip angle.

Figure 5.7 is a fringe plot of the maximum principle stress from the 2D FEA model. This plot is based on a 10 kip stringer load and the fringe plot displays a range of stress values from 14,000 psi to 34000 psi.

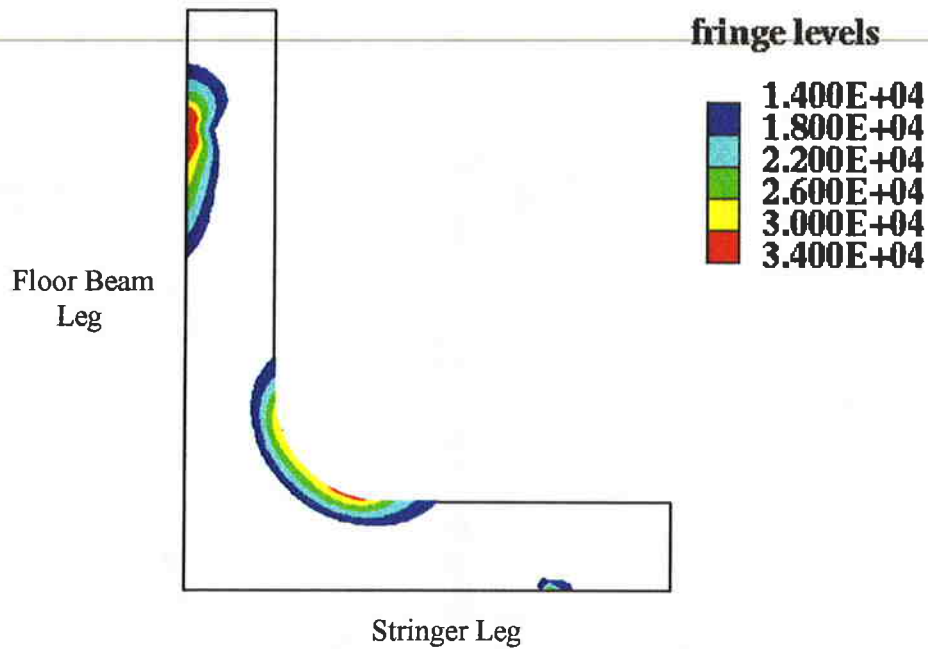


Figure 5.7 Fringe plot of the maximum principal stress for a interior panel clip angle from the 2D FEA model.

There are two areas that achieve peak stress levels. The first is located at the base of the clip angle where it is attached to the floor beam. This peak stress is not relevant because the riveted connections are simplified at that location. The other peak stress area is located at the root of the fillet on the stringer leg.

The fixed rotation model of the floor beam is used to model the clip angles attached to interior floor beams. The fixed top flange model of the floor beam is used to model the clip angles attached to floor beams at the end of the span. Figure 5.8 is a fringe plot of the maximum principle stress for clip angles in the interior panels (fixed rotation model). Figure 5.9 fringe plot of the maximum principle stress for clip angles at the end of the span (fixed top flange model). In both cases, the stringer is loaded with 10 kip and the fringe plots display a range of stress values from 9000 psi to 17,000 psi.

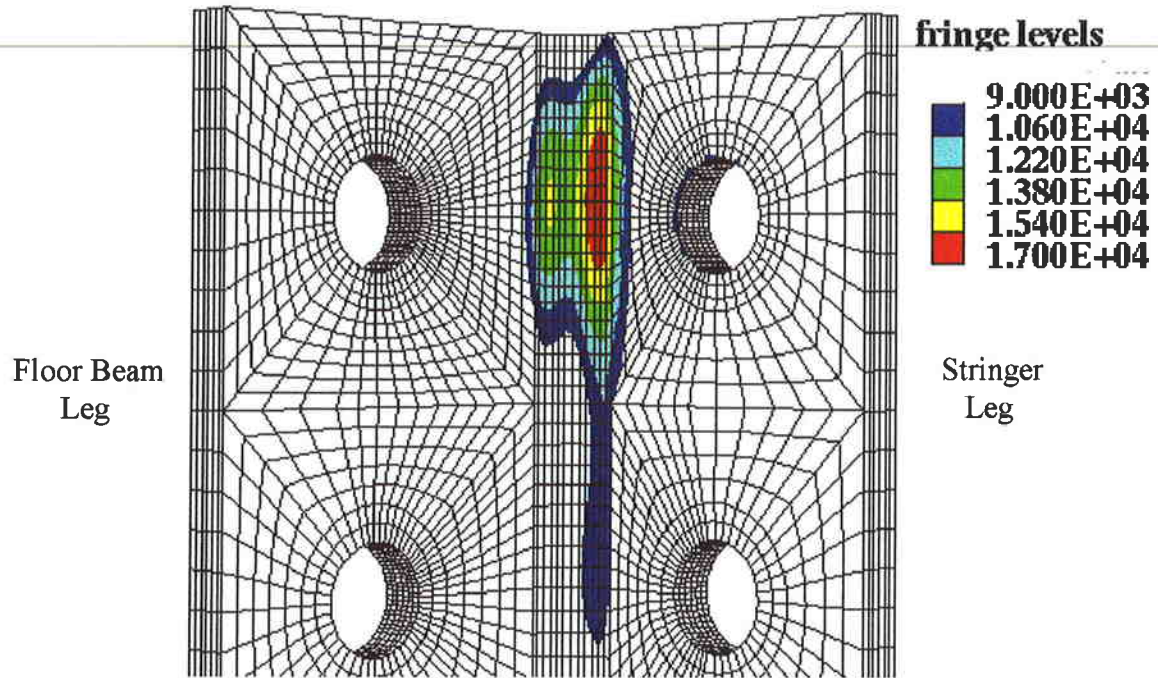


Figure 5.8 Fringe plot of the maximum principal stress from the 3D FEA model using the fixed rotation model of the floor beam.

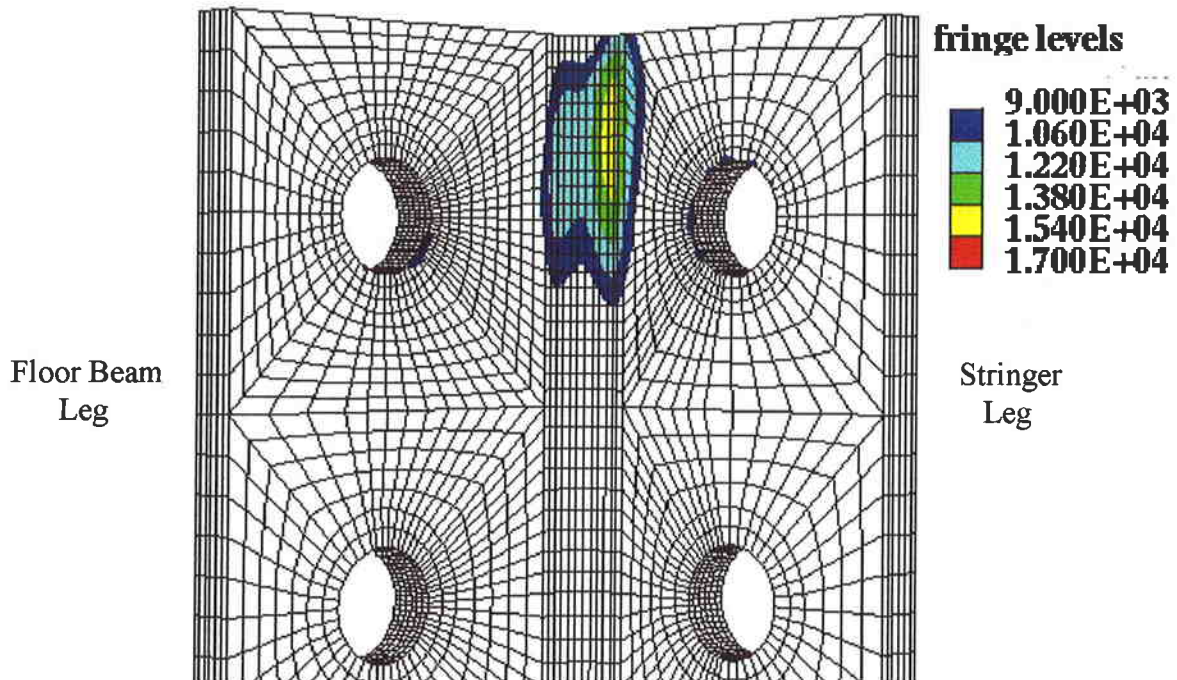


Figure 5.9 Fringe plot of the maximum principal stress from the 3D FEA model using the fixed top flange model of the floor beam.